Available online at www.sciencedirect.com
ScienceDirect
Bioelectrochemistry 70 (2007) 421–434
Bioelectrochemistry
www.elsevier.com/locate/bioelechem

Probing organization and communication at layered interfaces

Monika Dominska [a], Maciej Mazur [b], Kelly P. Greenough [a], Monique M. Koan [a], Paweł G. Krysiński [b], G.J. Blanchard [a,*]

[a] *Michigan State University, Department of Chemistry, East Lansing, MI 48824, USA*
[b] *University of Warsaw, Faculty of Chemistry, Pasteura 1, Warszawa 02-093, Poland*

Received 28 December 2005; received in revised form 20 February 2006; accepted 22 June 2006
Available online 27 June 2006

Abstract

We have investigated the local organization intrinsic to a variety of interfacial structures, by both electrochemical and spectroscopic means. Our focus has been on the design and construction of biomimetic interfaces, where a lipid bilayer or a hybrid bilayer membrane can be bound to an interface. The goal of this work is ultimately to create an interface on a transducer surface that can support an enzyme in its active form. To this point, we have examined the extent of organization that is achievable in monolayers that will be used to bind bilayer structures to a transducer surface. Our electrochemical data point to the important role of the substrate surface in determining adlayer organization. We have also investigated the fluidity and structural heterogeneity of lipid bilayers using time-resolved and steady state fluorescence spectroscopy. Our data point to the highly interactive nature of lipid bilayer constituents, where perturbations introduced to one region have significant consequences on other regions of the bilayer. Such information is directly relevant to the existence and properties of lipid raft structures in both model and biological bilayers.

Keywords: Surface-modification; Interfacial electron transfer; Unilamellar vesicles; Fluorescence anisotropy

1. Introduction

Developing sensors that can take advantage of the inherent selectivity of biomolecules holds great appeal. With any sensing device, there are two essential components; the chemically or biologically selective interface between the device and the outside world, and the non-selective transducer that takes the signal of interest generated chemically or physically, and converts that signal into a readable quantity, typically either electrons or photons. For this reason most transducers, which function as the substrate on which the selective adlayer resides, are polar, and it is not possible to deposit biomolecules directly onto the sensing transducer and expect them to retain their activity. We have been investigating ways to provide an interfacial medium for biomolecules that will allow these molecules to remain in their active state after deposition and thus function as the chemically or biologically selective element in our sensors.

To this point, we have not created a working sensor based on biomolecular selectivity. We have focused on the fundamental structural and chemical properties of the interfaces on which the biomolecules will be supported, and we discuss our progress to date in this paper. There are two distinct parts to this work. The first is the electrochemical and spectroscopic probing of the interfaces we form on metal and oxide surfaces using covalent bonding chemistry. The second is the spectroscopic interrogation of lipid bilayer structures to determine how the composition of these bilayers affects their dynamical properties. These bodies of information, taken collectively, provide insight into the parameters that are important in designing a functioning, surface-mounted biomimetic system.

We use a variety of well established chemical bonding schemes, ranging from thiol chemistry for bonding to Au [1–3] to covalent bonding to oxide surfaces such as indium-doped tin oxide (ITO) or silica (SiO_x) [4,5]. We have designed a series of SAMs that contain pyrene derivatives. Pyrene is a well known chromophore used to characterize local "polarity", and both its time- and frequency-domain spectral properties are sensitive to short range organization

* Corresponding author. Tel.: +1 517 355 9715x224.
E-mail address: blanchard@chemistry.msu.edu (G.J. Blanchard).

1567-5394/$ - see front matter © 2006 Elsevier B.V. All rights reserved.
doi:10.1016/j.bioelechem.2006.06.002

[6–15]. The electrochemistry of pyrene is also well understood, particularly with respect to its oxidative instability [16]. Interrogating both the spectroscopic and electrochemical behavior of covalently bound pyrene on metallic and oxide substrates provides information on the local organization of the interface. We use silica as the substrate for our spectroscopic experiments. The surface of silica is different from that of ITO, but earlier work has indicated that the density and distribution of surface –OH groups on these two substrates is similar [16]. The data we report here indicate that monolayers formed on silica and ITO are significantly disordered.

We have also examined the properties of the bilayers we intend to deposit onto the modified surfaces. These biomimetic adlayers are in the form of unilamellar vesicles. We have used NBD hexanoic acid (NBDHA), an NBD-tagged cholesterol (NBD-cholesterol) and a rhodamine-tagged phospholipid (DMPE-rhodamine) (Fig. 1) as chromophores in this work. Our choice of chromophores is based on the location on/in the bilayer structures where the chromophores will localize. We expect that NBD-cholesterol will associate with the cholesterol-rich regions of the bilayer, DMPE-rhodamine will locate in the lipid regions. For NBDHA, we find that the chromophore experiences the same environment regardless of vesicle composition or the specific phospholipid used, pointing to it residing in close proximity to the head group region of the vesicles.

Using NBD-cholesterol and DMPE-rhodamine, we have studied how chromophore dynamics are influenced by bilayer composition. We have systematically varied the amount of sphingomyelin and chromophore(s) present in these vesicles, and have monitored variations in the fluorescence lifetime and anisotropy behavior of the chromophores as a function of vesicle composition. The addition of cholesterol and sphingomyelin (SPM) to phospholipid vesicles is known to induce phase segregated regions within the bilayer structures [17]. SPM is thought to interact preferentially with cholesterol, leading to the formation of phase separated regions within the bilayer. Our data show that SPM does not play an easily measurable role in mediating bilayer organization, but the presence of chromophores in these bilayers can alter the fluidity of the bilayers themselves. While any bilayer constituent can cause structural perturbations, the identity and location of the constituent both play important roles in determining the precise perturbation. Our data underscore the highly cooperative nature of bilayers, where perturbations in one region

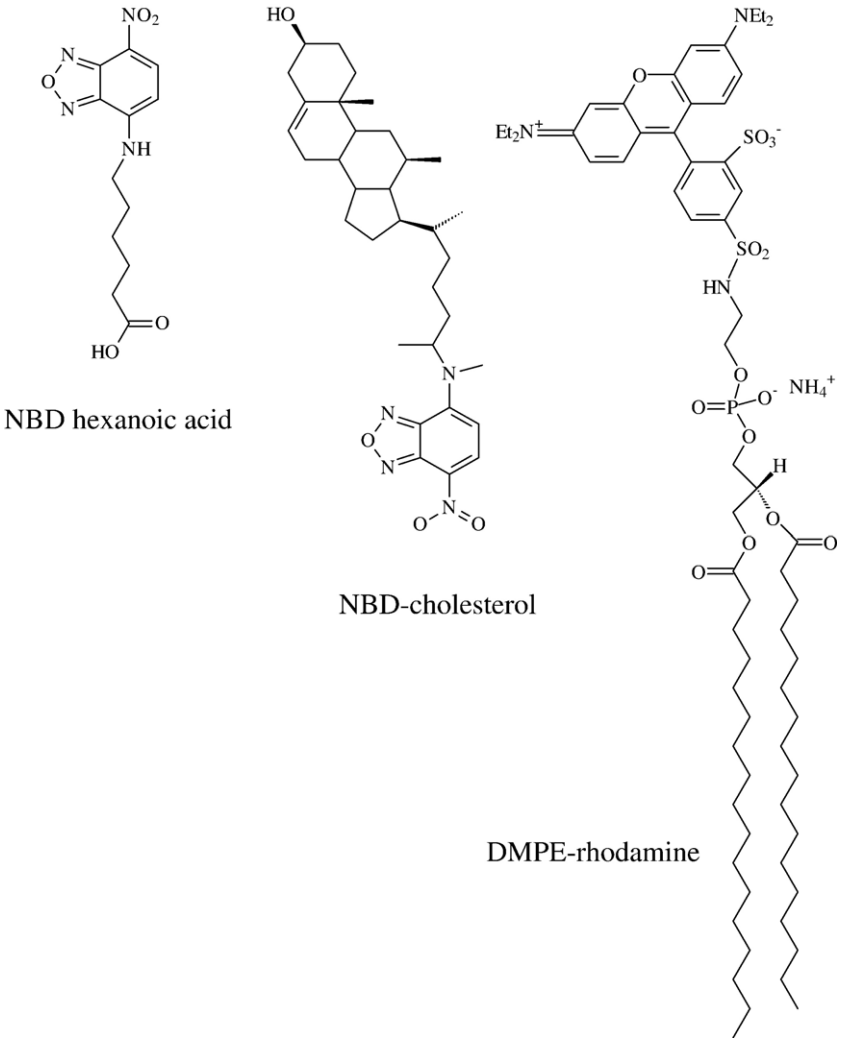

Fig. 1. Structures of chromophores used to probe unilamellar vesicle structure.

of the bilayer can have measurable consequences in different regions.

2. Experimental section

2.1. Chemicals

1-Pyrenebutyric acid (97%), 1-pyrenemethylamine hydrochloride (95%), octadecylamine (97%), 2-mercaptoethylamine (95%), 11-mercaptoundecanoic acid (95%), 10-hydroxydecanoic acid, octadecylmercaptan (98%), 1-hexadecylamine (98%), *N*,*N*′-dicyclohexylcarbodiimide (DCC) (99%), adipoyl chloride (≥99%), 4-methylmorpholine (≥99.5%), triethylamine (≥99%), perchloric acid (70%), ruthenium (III) hexamine chloride (98%), potassium ferrocyanide (99%), lithium perchlorate (99.99%), cyclohexane (99%), 1-pentanol (≥99%), acetonitrile (anhydrous) were obtained from Aldrich. Dichloromethane and chloroform were obtained from POCH or from Mallinckrodt Chemicals. Aqueous solutions were prepared from Milli-Q water.

For the vesicle bilayer studies, the fluorescent probe 6-(*N*-(7nitrobenz-2-oxa-1,3-diazol-4-yl)amino hexanoic acid (NBDHA) was obtained from Molecular Probes Inc. and used without further purification. The solvents methanol, 1-propanol, 1-butanol, 1-pentanol, dimethyl sulfoxide (DMSO), *N*,*N*-dimethylformamide (DMF) and acetonitrile were purchased from Sigma-Aldrich in their highest purity available. Water and ethanol (95%) were distilled in-house. The concentration of NBDHA in solvents and the concentration of NBDHA in the vesicles for one-photon experiments was 10^{-5} M, while the concentration of NBDHA in vesicles for two-photon excitation experiments was 10^{-4} M. Powdered cholesterol, 1,2-dimyristoyl-*sn*-phosphatidylcholine (DMPC), egg sphingomyelin (SPM), 25-(*N*-(7-notrobenz-2-oxa-1,3-diazol-4-yl-methyl) amino)-27-norcholesterol and 1,2-Dimyristoyl-*sn*-Glycero-3-Phosphoethanolamine-*N*-(Lissamine Rhodamine B Sulfonyl Ammonium Salt), (DMPE-Rhodamine) were purchased from Avanti Polar Lipids Inc., and used without further purification.

2.2. Substrate preparation

For the electrochemistry experiments, gold ball electrodes were cleaned in piranha solution (3:1 concentrated H_2SO_4/30% H_2O_2), rinsed with water and polarized cyclically (scan rate 100 mV/s) from −250 mV to +1650 mV in 1 M $HClO_4$ until reproducible voltammograms were obtained. The area of the gold ball electrode was 0.135 cm^2, determined from the cyclic voltammetry of a $K_4[Fe(CN)_6]$ solution [18]. Silica slides were cleaned by immersion in piranha solution for ca. 20 min, then rinsed with water and dried in a stream of nitrogen. Indium-doped tin oxide (ITO) films deposited on silica substrates were cleaned by rinsing with water, ethanol and acetone, consecutively.

2.3. Monolayer preparation

Pyrene bound to gold using a "short tether" (the cysteamide of pyrenebutyric acid, P7, the number 7 indicates the number of atoms between the substrate-attaching head group and the pyrene chromophore) was synthesized according to a procedure for solution-phase peptide synthesis [19]. To create a monolayer of P7 on gold, the substrate was exposed to solution of P7 in dichloromethane for 12 h. The monolayer of the nominally buried P7 was obtained by immersing a gold electrode into a solution of P7 and octadecyl mercaptan (ODM) (1:1) in dichloromethane for 12 h. For deposition of a monolayer of pyrene tethered a greater distance from the gold substrate, the substrate was first exposed to solution of 11-mercaptoundecanoic acid (MUA) in dichloromethane for 12 h. The resulting SAM-covered gold substrate was rinsed with dichloromethane, dried in a stream of nitrogen and immersed in a solution of pyrenemethylamine and DCC (1:1) in dichloromethane for 12 h, to form a monolayer of mercaptoundecanoic acid pyrenemethylamide (P13). To synthesize a monolayer of "buried" P13, a substrate covered with a monolayer of 11-mercaptoundecanoic acid (MUA) was immersed in a dichloromethane solution containing pyrenemethylamine, hexadecylamine and DCC (1:1:1) for 12 h.

Monolayers on ITO and SiO_x substrates were synthesized by reaction of the substrate with adipoyl chloride (0.3 mL) in dry acetonitrile (10 mL), using 4-methylmorpholine (0.3 mL) as a Lewis base, under reduced pressure for 1 h, followed by rinsing with dry acetonitrile and ethyl acetate, and drying under a stream of dry nitrogen. We synthesized monolayers of tethered pyrene either as the only constituent or as a co-constituent with a long-chain aliphatic moiety. These monolayers were obtained by exposing the adipoyl chloride covered substrate either to a 2 mM solution of pyrenemethylamine in dichloromethane, producing a single-component monolayer of the pyrenemethylamide of adipic acid, P8. For the corresponding monolayer where P8 is "buried", a dichloromethane solution of pyrenemethylamine and hexadecylamine (1:1) is reacted under reduced pressure for 0.5 h. For pyrene tethered further from the substrate, the adipoyl chloride covered substrate was first reacted with a 2 mM solution of 10-hydroxydecanoic acid in dichloromethane. Following the addition of this C_{10} chain, the substrate was removed from the reaction vessel, rinsed with dichloromethane and ethyl acetate, and dried under a stream of dry nitrogen. The substrate thus covered with adipic acid mono-(10-carboxy)-decyl ester was then exposed either to pyrenemethylamine and DCC (1:1) to form pyrenemethylamide-10-decyl ester, (P19) in dichloromethane or to pyrenemethylamine, hexadecylamine and DCC (1:1:1) in dichloromethane under reduced pressure for 0.5 h.

2.4. Unilamellar vesicle formation

For the construction of unilamellar vesicles, the lipids 1,2-Dilauroyl-*sn*-Glycero-3-Phosphocholine (DLPC, mp=−1 °C), 1,2-Dimyristoyl-*sn*-Glycero-3-Phosphocholine (DMPC, mp=23 °C), 1,2-Distearoyl-*sn*-Glycero-3-Phosphocholine (DSPC, mp=55 °C), egg sphingomyelin (SPM) and powdered cholesterol were obtained from Avanti Polar Lipids, Inc. For the NBDHA experiments, vesicle constituents were prepared in a 1:1:1 mole ratio of phospholipid/cholesterol/sphingomyelin or a 2:1 mole ratio of phospholipid/cholesterol for the multicomponent

systems. For the mixed lipid systems, the ratio of phospholipids used was 1:1. A total of nine vesicle systems were produced with varying composition. The vesicle compositions were as follows: DLPC, DLPC/cholesterol, DLPC/cholesterol/SPM, DSPC, DSPC/cholesterol, DSPC/cholesterol/SPM, DLPC/DSPC, DLPC/DSPC/cholesterol, and DLPC/DSPC/cholesterol/SPM. Chloroform was evaporated from the lipid solutions, then the vesicle constituents were dissolved in a 4:1 benzene:methanol solvent system, followed by another evaporation. The resulting lipid mixture was then dissolved in a 10 mM solution of Tris® buffer (Aldrich) in Milli-Q water. The Tris® buffer was adjusted for a pH ~8. An equal volume of the NBDHA-containing solution (2×10^{-4} M) was added next for a final total concentration of the vesicle constituents of 1 mg/mL, and 10^{-4} M in NBDHA. Mixing of the solution was accomplished by freeze–thaw–vortex cycles, described below.

For BBD-cholesterol and DMPE-rhodamine experiments, the lipids (DMPC, SPM), cholesterol, and optical probes were mixed in selected ratios and the chloroform solvent was evaporated. The samples all contained a total concentration of 33 mol% cholesterol (the sum of 32.5 mol% powdered cholesterol and 0.5 mol% NBD-cholesterol) with a varied concentration of SPM (0, 11, 22 and 33 mol%) and DMPE-Rhodamine (0–1.00 mol%). The balance of the vesicle was comprised of the phospholipid. The mixtures were processed five times through a freeze–thaw–vortex cycle to ensure complete mixing. After the freeze–thaw–vortex process, the solutions were extruded once through polycarbonate membrane filters with a 400 nm pore diameter using a mini-extruder (Avanti Polar Lipids Inc.). The initial vesicle suspension was then extruded 11 times through polycarbonate membranes (Avanti Polar Lipids Inc.) with a nominal pore diameter of 100 nm. The resulting solution contained vesicles with a size distribution centered around 100 nm (Fig. 2) [20–25].

2.5. Electrochemistry

Electrochemical measurements were made with a computer-controlled Electrochemical Workstation (CH instruments Model 604B and Model 650), using a three-electrode cell with a Pt wire counter electrode. All potentials are quoted versus a Ag/AgCl/1 M KCl_{aq} reference electrode. Experiments were carried out in aqueous 0.01 M, 0.05 M, 0.1 M, 0.5 M and 1 M $HClO_4$ (keeping the 1 M ionic strength constant by adding $LiClO_4$), in aqueous 1 mM $K_4[Fe(CN)_6]$ in 0.5 M $LiClO_4$, and in aqueous 1 mM $[Ru(NH_3)_6]Cl_3$ in 0.1 M $LiClO_4$.

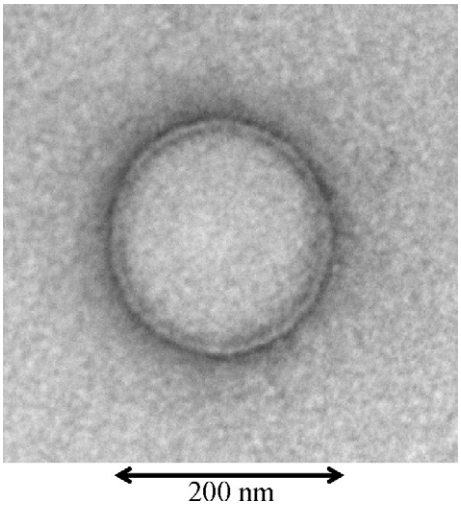

Fig. 2. TEM image of unilamellar vesicles produced by extrusion.

2.6. Time-resolved emission measurements

Time-correlated single-photon counting (TCSPC) was used to study the lifetime and motional relaxation properties of the chromophores used here. The TCSPC system used to acquire time-domain data has been described elsewhere [26] and is reviewed briefly here. The second harmonic or third of the output of a mode-locked CW Nd:YAG laser (Coherent Antares 76-S) is used to excite a cavity-dumped dye laser (Coherent 702-2) operated at 640 nm using Kiton Red laser dye (532 nm excitation, Exciton), at 580 nm with Pyromethene 567 dye (532 nm excitation, Exciton), or at 430 nm using Stilbene 420 dye (355 nm excitation, Exciton). The output of the dye laser was ≤100 mW average power at 4 MHz repetition rate with ~5 ps pulses. The light incident on the sample is either the fundamental or its second harmonic generated by frequency doubling the dye laser output using a Type I $LiIO_3$ SHG crystal. The average optical power at the sample is less than 1 mW. The detection electronics are characterized by an instrument response function of 35 ps fwhm. The emission collection wavelength and polarization are computer controlled using National Instruments LabVIEW® v. 7.0 software.

2.7. Steady state spectroscopy

The absorption spectra were obtained using a Cary 300 UV–visible spectrophotometer. Quartz cuvettes with a 1 cm pathlength were used for all measurements. Background samples without the fluorophore were used for baseline correction because of scattering from the vesicle-containing solutions. Steady state fluorescence measurements were performed using a SPEX Fluorolog-3 spectrophotometer using 1 cm pathlength quartz cuvettes. Excitation and emission slits with a nominal bandpass of 3 nm were used for all experiments.

2.8. Transmission electron microscopy

Samples were fixed with a 2% osmium tetroxide solution in 0.1 M cacodylate buffer (pH ~7.4). TEM images of the vesicles (Fig. 2) were acquired using a JEOL 100CX TEM operated at an accelerating voltage of 100 kV.

3. Results and discussion

3.1. Organization in surface-bound monolayers

We have investigated pyrene derivatives bound covalently to gold and ITO substrates by cyclic voltammetry, and these same compounds bound to SiO_x by optical spectroscopy. The cyclic voltammograms (CVs) of the tethered pyrene derivatives bound to

gold and ITO are shown in Fig. 3. In the first scan for each voltammogram there is an irreversible peak with a maximum above 900 mV. A pair of new, broad redox peaks appears in subsequent scans in the range of 200 to 350 mV. These peaks are assigned to 1,6-pyrenedione/1,6-dihydroxypyrene (a pair of CV peaks centered around 0.32 V), and 1,8-pyrenedione/1,8-dihydroxypyrene, which is shifted to more negative values by ca. 100 mV [16,27]. The electrode coverage with various pyrene derivatives was also evaluated using CV. We calculate a surface coverage (for a $2e^-/2H^+$ reaction) of 4.4×10^{-11} mol/cm^2 for P7 and 1.7×10^{-11} mol/cm^2 for P13. On ITO we recover surface coverages of 1.2×10^{-11} mol/cm^2 for P8 and 8.4×10^{-12} mol/cm^2 for P19. We estimate the "footprint" of a single pyrenebutyric acid molecule to be 31.2 Å^2 [28] intermediate between that of an alkanethiol (25 Å^2/mlc.) [37] and cholesterol in a monolayer (37 Å^2/mlc.) [29]. The maximum theoretical surface coverage of pyrene on a flat electrode surface is 5.3×10^{-10} mol/cm^2, indicating that our experimental surface coverages are a fraction of a monolayer.

Considering the sub-monolayer coverage of our SAMs and consequent accessibility of the electrode surface, and the role of protons in these redox reactions (scheme 1), we expect a pH dependence in the midpoint potential, E_m. Between E_{pa} and E_{pc}, a gradual decrease in pH should lead to a shift of the midpoint potential by ca. 60 mV per pH unit if the ratio of protons to electrons is one ($2H^+$, $2e^-$). The experimental data show that the pH dependence of the midpoint potential, E_m, is ca. −45 mV/pH unit (Fig. 4a,b) for P7 and P13 on gold, and ca. −50 mV/pH unit for P8 and P19 on ITO (Fig. 4c,d). It appears that the pyrene derivatives on either Au or ITO do not undergo a full $2H^+/2e^-$ redox reaction. The experimental H^+/e^- ratio is ca. 0.8, similar to that for the ubiquinone/ubiquinol (UQ/UQH_2) redox couple on a mercury surface by a phospholipid monolayer [30–32].

We use AC voltammetry to quantitate the redox kinetics of the surface-bound pyrene derivatives. This technique is particularly useful for investigating redox reactions in layered assemblies on electrodes [33–36], owing to the range of information available from such data. For a reversible reaction, the peak potential values are smaller by ca. 58 mV than the formal potential values obtained during the CV experiments. For AC voltammetry, the difference in peak position between P13 and P7 is slightly higher than that obtained from dc CV, yielding a $\Delta(\Delta G^0)$ value of ca. 7 kJ/mol.

We observe a decrease in the peak-to-background current ratio with increasing frequency (Fig. 5a), reflecting the rate constant of the reaction. We have used Creager's method [33–35] to analyze these data and show the frequency-dependence of the AC data in the form of the peak current to background current ratio, I_p/I_b vs. log(AC frequency) (Fig. 5b). The recovered rate constants from fits of the model to the data are $k_{ct}=1200\ s^{-1}$ for P7 and $25\ s^{-1}$ for P13. It is useful to consider the differences in rate constant values for P7 and P13 in terms of through-bond tunneling that should depend exponentially on the distance and/or the number of C − C

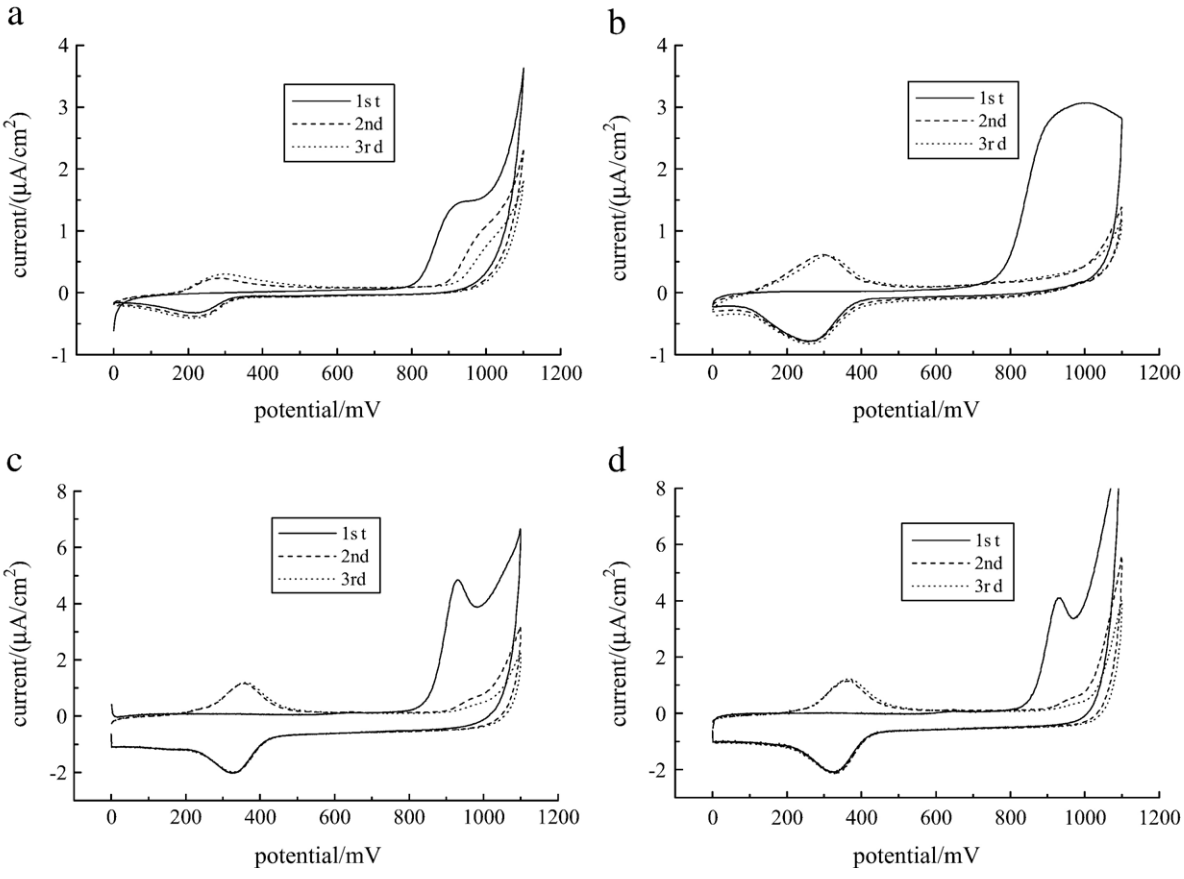

Fig. 3. Cyclic voltammograms of (a) P7 on gold in 0.1 M $HClO_4$, sweep rate 2 mV/s. (b) P13 on gold in 0.1 M $HClO_4$, sweep rate 5 mV/s. (c) P8 on ITO in 1 M $HClO_4$, sweep rate 20 mV/s. (d) P19 on ITO in 1 M $HClO_4$, sweep rate 20 mV/s.

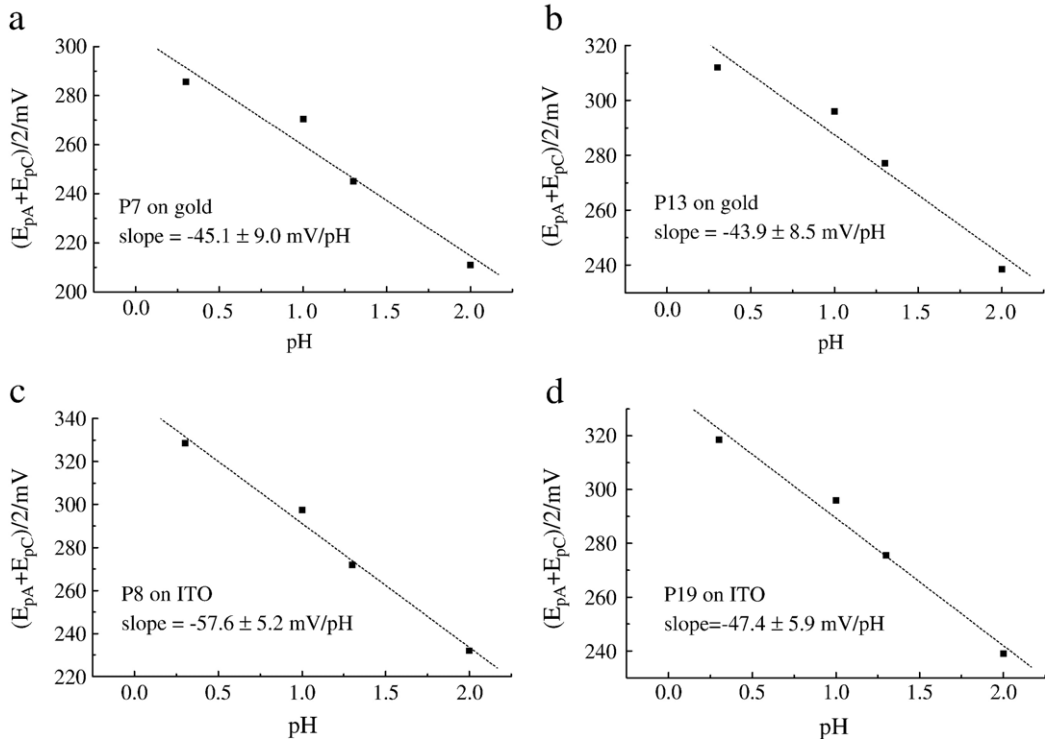

Fig. 4. Dependence of the midpoint potential, E_m, on the pH of perchloric acid aqueous solutions for (a) P7 on gold, slope=−45.1±9.0 mV/pH, (b) P13 on gold, slope=−43.9±8.5 mV/pH, (c) P8 on ITO, slope=−57.6±5.2 mV/pH, and (d) P19 on ITO, slope=−47.4±5.9 mV/pH. For all scans the sweep rate was 20 mV/s. Uncertainties indicated in all panes are $\pm 1\sigma$.

bonds in the anchoring chain. Assuming typical bond lengths (1.79 Å for the C − S bond, 1.27 Å for each C − C bond and 2.6 Å for the amide group) [37], we obtain the tunneling constant, β from the experimental k_{ct} values:

$$1n = \left(\frac{k'_{ct}}{k''_{ct}}\right) = \beta(d'' - d') \quad (1)$$

where k'_{ct} and d' are rate constant and chain length of P7 and k''_{ct} and d'' are the rate constant and chain length of P13. The use of a single tunneling constant, β, for different length anchoring chains requires justification. The tether molecules, aside from their length, vary in the position of the amide group and the pyrene ring system relative to the substrate. The contribution of an amide group to the electronic coupling is thought to be approximately that of two methylene groups [38,39]. Due to the structural similarities of P7 and P13, we assumed the same tunneling constant for both molecules bound to the electrode surface. For P7 and P13 bound to gold, Eq. (1) yields a value of β=0.44/Å, approximately half the literature value of 0.85/Å for a polymethylene chain [40]. For a P13 monolayer on gold, the chemical system is much more complex than the Randles equivalent circuit implies and fitting the data using a single rate constant is an over-simplification. Our results suggest some disorder in the structure of these monolayers, leading to a distribution of rate constants and β values.

We have acquired the analogous AC voltammetry data and performed the same analysis for P8 and P19 on ITO. Analysis of these data in the same manner yields much smaller k_{ct} values that depend weakly, if at all, on the anchoring chain length (k_{ct}=0.2 s^{-1} for P8 and 0.1 s^{-1} for P19). We assume that the ester groups present on the tether chains reduce the rate of electron transfer analogous to that seen for ether groups [41], making through-chain electron transfer inefficient. If this is in fact the case, the contribution of intermolecular interactions to the electron transfer process may become significant. Such a contribution could result from a highly disorganized adlayer, where the tethers of the pyrene derivatives as well as the pyrene rings form disorganized aggregates, thereby maintaining the pyrene ring system at roughly the same average distance from the electrode surface for both P8 and P19. For the pyrene derivatives attached to ITO, we extract a value of +328 mV for the formal potential, in agreement with the value of +324 mV obtained for a similar aminomethylpyrene derivative tethered to gold.

3.2. Pyrene derivatives surrounded by aliphatic chains

We consider next interfaces where the pyrene ring system is present in an adlayer comprised of mostly aliphatic species. These mixed monolayers contain the same pyrene derivatives as discussed above, but they are co-adsorbed with “diluent” molecules of longer hydrocarbon chains. Octadecanethiol was the diluent for monolayers containing P7 and the hexadecylamide of mercaptoundecanoic acid was the diluent for monolayers containing P13 on gold substrates. Adipoylhexadecylamide was used as the diluent for monolayers containing P8 and the mono-(9-carboxy)-nonyl ester of adipic acid hexadecylamide was the diluent for monolayers containing P19 on ITO. The co-adsorbed diluent molecules do not improve the organization and passivation

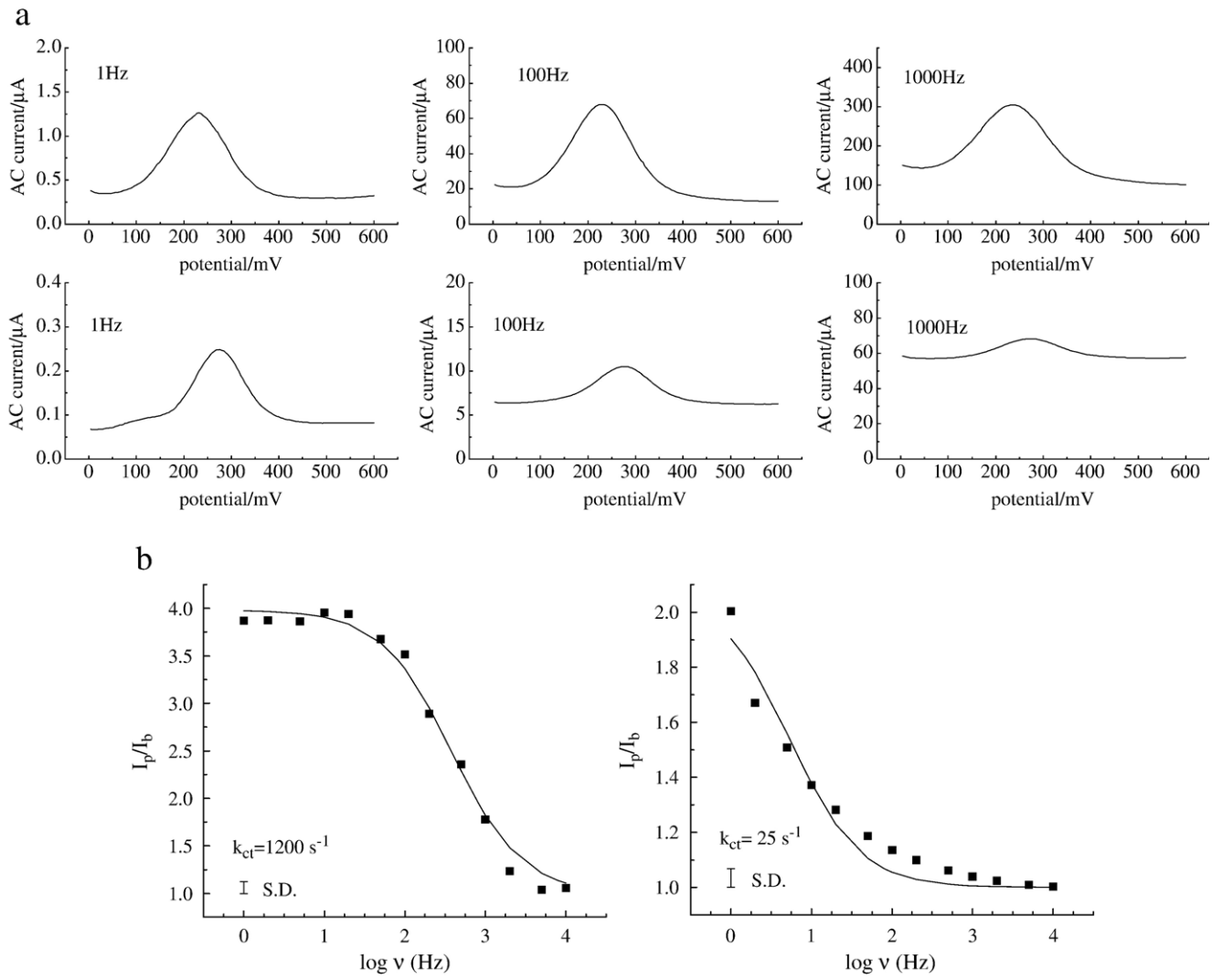

Fig. 5. (a) AC voltammograms for P7 (top row) and P13 on gold in 0.1 M $HClO_4$. AC frequencies are indicated in each pane. (b) $I_{peak}/I_{background}$ vs. log(frequency) plots of monolayers of P7 (left) and P13 (right) on gold; The solid lines represent fits to the data (black squares) using a Randles equivalent circuit [33–35].

properties of the mixed monolayers compared to the one-component interfaces. For gold electrodes we recover a surface coverage of 3×10^{-11} mol/cm^2 for P7 diluted with octadecanethiol and 4×10^{-12} mol/cm^2 for P13 diluted with mercaptoundecanoic acid hexadecylamide. For ITO, we obtain a coverage of 8.4×10^{-12} mol/cm^2 for P8 diluted with adipoylhexadecylamide and 5.5×10^{-12} mol/cm^2 for P19 diluted with the mono-(9-carboxy)-nonyl ester of adipic acid hexadecylamide.

The AC voltammetry experiments for these systems illustrate that when the pyrene ring system is confined within a mixed monolayer interior, the AC current peak disappears at much lower frequencies than for the corresponding one-component monolayer. The kinetics of charge transfer are slower for the two-component system, and we extract $k_{ct}=1100$ s^{-1} for P7+diluent and 21 s^{-1} for P13+diluent on gold. These data show that the presence of diluent chains slightly improves the spatial organization of pyrene rings within the monolayer.

Analogous experiments for ITO-supported adlayers show that the charge transfer kinetics of pyrene derivatives follow the same pattern. The charge transfer rate constants for P19 (0.1 s^{-1} without diluent, 0.008 s^{-1} with diluent) and for P8 (0.2 s^{-1} without diluent, 0.08 s^{-1} with diluent), also indicate structural confinement and improved organization due to the presence of the aliphatic diluents.

3.3. Spectroscopic characterization of tethered pyrene on SiO_x

We have used pyrene as an optical probe because we understand its photodegradation behavior and because its emission spectrum is known to be sensitive to the "polarity" of its local environment [6–15]. We use the same reaction chemistry to modify silica and ITO surfaces. While these surfaces are certainly not identical, their reactivities toward acid chlorides and other compounds such as $POCl_3$ are very similar. It is difficult to make direct comparisons between the interfaces because they are not amenable to probing by the same means. We can estimate from absorbance data that the surface PAH concentrations on these two materials are similar, and neither material exhibits mesoscopic crystallinity. These pieces of information suggest that whatever the

organization of the chromophores on these interfaces, it is likely similar, and it is on this basis that we detail the spectroscopic characterization of a series of pyrene derivatives tethered to silica.

The steady state absorption and emission spectroscopy of pyrene is well understood. The emission data for tethered pyrene derivatives provide information about the organization and polarity of these interfaces, and we utilize both time domain and frequency domain data.

We show in Table 1 the pyrene I/III emission band ratios, a quantity related to environmental polarity, for pyrene in the solvents used here. We also show the I/III emission band ratios for the surface-bound derivatives in a nitrogen atmosphere and immersed in the solvents cyclohexane, 1-pentanol and water. For solution phase pyrene, we obtain the expected polarity dependence, with the I/III band ratio being largest for water (most polar) and smallest for cyclohexane (least polar). For the tethered derivatives we observe the maximum I/III band ratios for immersion in 1-pentanol, and a decrease in I/III ratio for immersion in water. P19 does not quite follow this trend, although it is apparently in a comparatively nonpolar environment. For the substrate-bound species, the water overlayer causes the interfacial adlayer to "fold over" and become disorganized, with the pyrene chromophore seeking an environment that is relatively non-polar. For 1-pentanol, the modified interfaces can be solvated effectively and the pyrene is thus exposed to the solvent to a greater extent than it is for the water overlayer. The cyclohexane data show similar I/III band ratios for the solution phase and surface-bound species, suggesting relatively effective solvation of the interface by this nonpolar solvent. Taken collectively, these data suggest that the presence of water above the interface gives rise to significant disorganization of the adlayer, and this finding is consistent with the electrochemical information presented above as well as the time-domain emission data we consider next.

The time-resolved emission response of pyrene and its derivatives has been studied extensively [15]. For the native chromophore, the dominant excitation is for the $S_2 \leftarrow S_0$ transition and emission is from the S_1 state. These states are polarized orthogonal to one another, leading to negative anisotropy values. For substituted pyrene derivatives, the addition of some chemical functionality to the pyrene ring structure perturbs the electronic states to an extent that depends on the identity of the substitution. In some cases this perturbation leads to the two electronic states being polarized at an angle less than 54.7° with respect to one another, and it other cases, the polarization difference between the two states remains at a value greater than 54.7° [42–45]. For the substituted pyrene derivatives we use, we observe a positive anisotropy signal.

Table 1
Steady state band intensity ratios for surface-bound pyrene derivatives as a function of the solvent in which these interfaces are immersed

Medium	Dipole moment (D)	Dielectric constant (ε_0)	I/III band intensity ratios				
			Pyrene[a]	P8	P8+ diluent	P19	P19+ diluent
Nitrogen			–	0.68	0.78	0.74	0.79
Cyclohexane	0.00	2.02	0.58	0.71	0.76	0.81	0.75
1-Pentanol	1.65	13.9	1.02	1.01	1.27	1.06	1.25
Water	1.85	78.5	1.87	0.95	1.03	1.09	0.94

[a] Experimental values for pyrene from Dong and Winnik treatment [6,7].

Table 2
Summary of time-resolved data for P8 and P19 on silica

Medium		Monolayer composition			
		P8	P8+diluent	P19	P19+diluent
Air	τ_{rot} (ps)	224±49	174±30	–	–
	$R(0)$	0.12±0.02	0.30±0.04	0.03±0.01	0
	$R(\infty)$	0.02±0.01	0.21±0.01	0.03±0.01	0
Water	τ_{rot} (ps)	81±25	∞ (314±326)	–	–
	$R(0)$	0.11±0.02	0.03±0.02	0	0
	$R(\infty)$	0.08±0.01	0.02±0.01	0	0
Pentanol	τ_{rot} (ps)	453±13	537±30	397±24	–
	$R(0)$	0.20±0.01	0.22±0.01	0.24±0.01	0.05±0.01
	$R(\infty)$	0.03±0.01	0.04±0.01	0.04±0.01	0.05±0.01
Cyclohexane	τ_{rot} (ps)	71±42	319±67	–	–
	$R(0)$	0.10±0.04	0.21±0.03	0.09±0.01	0.10±0.01
	$R(\infty)$	0.03±0.01	0.11±0.01	0.09±0.01	0.10±0.01

We show in Table 2 the quantities τ, $R(0)$ and $R(\infty)$. These quantities are related to the experimental time-resolved intensity data $I_{\|}(t)$ and $I_{\perp}(t)$ through the following series of equations [46].

$$R(t) = \frac{I_{\|}(t) - I_{\perp}(t)}{I_{\|}(t) + 2I_{\perp}(t)} \tag{2}$$

$$R(t) = R(\infty) + (R(0) - R(\infty))\exp(-t/\tau) \tag{3}$$

$$\tau = \frac{7\theta_0^2}{24D_w} \tag{4}$$

$R(0)$ and $R(\infty)$ are the zero-time and infinite-time anisotropies, D_w is the "wobbling" diffusion coefficient, representing motion of the chromophore about its tether within a cone of semi-angle $2\theta_0$ [47]. The infinite time anisotropy is related to the average organization or extent of motional restriction experienced by the chromophore within its environment, and $R(0)$ is determined by the angle between the excited and emitting chromophore transition dipole moments. The quantities related to the organization of the interfacial structures are $R(\infty)$ and τ.

The $R(\infty)$ results for the interfaces containing P8 show that, in all cases, the interface is disorganized, with $R(\infty)$ values ranging from 0.02 to 0.08. For P8 co-adsorbed with longer organic adlayer species, we find a significantly smaller orientational distribution in air and cyclohexane, with $R(\infty)$ values for pentanol and water being consistent with a relatively disorganized interface (Table 2). For all of these measurements, save for P8 buried in an aliphatic environment, we see a decay of the anisotropy, and thus report a value of τ. Combining these data with the $R(\infty)$ results, we see that the local chromophore environment can place some motional restrictions on D_w. From the hindered rotor model,

$$R(\infty) = R(0)\langle P_2(\cos\theta)\rangle^2 \tag{5}$$

and we extract the quantities $R(\infty)$ and $R(0)$ from the experimental data (Fig. 6). If we assume that $\theta \sim \theta_0$ at long times, we can use

these data to provide information on both D_w and the intrinsic disorder in the films (Table 3). The entries marked"–" in Table 3 reflect the absence of detectable decay dynamics. The θ values in Table 3 are related to the free volume which the chromophore can access, and D_w is a measure of how rapidly the pyrene moiety is moving (rotating, wobbling) within that free volume.

P8 possess more motional freedom than P19. For P8, the cone angle θ is qualitatively similar for all interfaces immersed in solvent, and the D_w terms are significantly slower in the monolayer containing aliphatic diluent molecules, implying a more viscous environment [48]. P8 also exhibits a significant solvent-dependence to its relaxation dynamics. For P8 in air, D_w is intermediate between that for water and cyclohexane. For P8 without diluent, the monolayer structure appears to be solvated efficiently by cyclohexane. In air, the pyrene chromophore layer either interacts with its neighbors or the substrate, and such interactions would likely provide an environment that will impede the pyrene ring system motion more than the presence of a low viscosity nonpolar solvent. Water and pentanol solvent overlayers yield the lowest D_w values for the P8 monolayer. The relatively polar solvents cause the nonpolar pyrene to interact most strongly with its neighbors or the surface, in effect creating a reasonably viscous environment. For the monolayers containing P8+diluent,

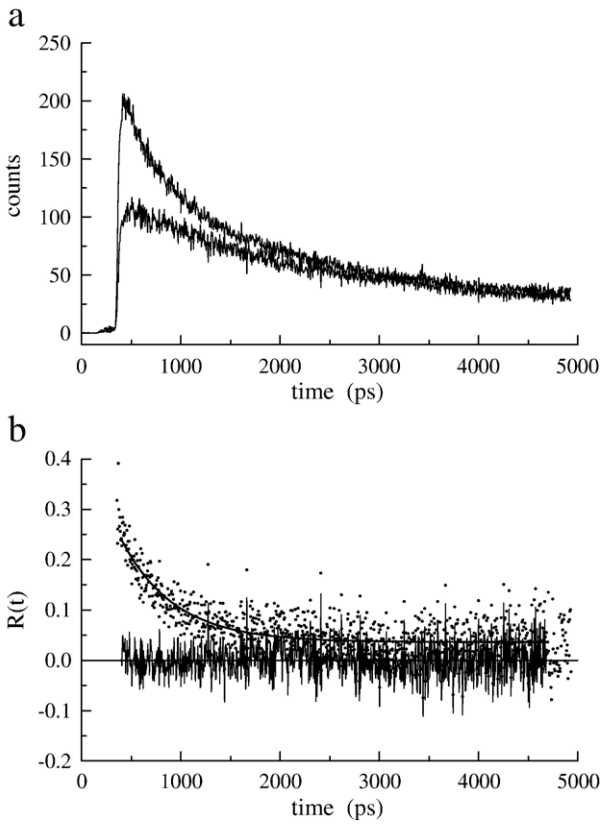

Fig. 6. (a) Time resolved emission intensities for emission polarizations parallel and perpendicular to the (vertical) excitation polarization for P8+ diluent bound to silica and immersed in 1-pentanol. (b) Induced orientational anisotropy function constructed from data shown in (a). The fit to the data and residuals are also shown.

Table 3
Results calculated for hindered rotor model

Medium		Monolayer composition			
		P8	P8+diluent	P19	P19+diluent
Air	θ (deg.)	39±9	19±4	–	–
	D_w (10^8 Hz)	6.0 (+11.6, −3.1)	1.80 (+1.5, −1.0)	–	–
Water	θ (deg.)	18±7	20±17	–	–
	D_w (10^8 Hz)	3.6 (+6.3, −2.6)	–	–	–
Pentanol	θ (deg.)	40±3	38±3	39±3	–
	D_w (10^8 Hz)	3.1 (+0.6, −0.5)	2.4±0.5	3.4 (+0.8, −0.7)	–
Cyclohexane	θ (deg.)	33±21	25±4	–	–
	D_w (10^8 Hz)	13.6 (+75, −12.5)	1.7 (+1.2, −0.7)	–	–

we observe some variation in θ but the values of D_w are solvent-independent to within the experimental uncertainty. The diluent thus provides a nonpolar environment for pyrene, isolating it from the polar solvent.

3.4. Bilayer dynamics and organization

We use unilamellar vesicles as model bilayer structures. The issues of primary concern are understanding the dynamics of bilayer constituents and what structural factors exert the most influence. We have used time-resolved and steady state spectroscopies to characterize three chromophores that localize to different portions of the intrinsically heterogeneous bilayer structures. We consider first the dynamics of NBDHA. For this chromophore, one-photon excited fluorescence anisotropy decays are single exponential. Based on Chuang and Eisenthal's treatment, the single exponential decay of $R(t)$ indicates that NBDHA is a prolate rotor with $\tau = 1/(6D_z)$ [49]. The one-photon reorientation times we recover are related directly to the viscosity of the local medium, as described by the modified Debye–Stokes–Einstein (DSE) equation [48,50,51]

$$\tau_{OR} = \frac{\eta V f}{k_B T S} \tag{6}$$

where η is the solvent bulk viscosity, V is the solute hydrodynamic volume $V_{NBDHA} = 245$ Å^3 [52], f is the frictional solvent–solute boundary condition, and S is the solute shape factor. There is a potential ambiguity in determining the Cartesian components of D based on the axis along which the excited transition moment is oriented [53]. To resolve this ambiguity, we have measured the transient fluorescence anisotropy of NBDHA using two-photon excitation. Reorientation data acquired using two-photon excitation produce anisotropy decay times are not related to the viscosity of the local medium in the same way as data for one-photon excitation, but are a permutation of the Cartesian components of D, the rotational diffusion constant, and the two-photon tensor elements. If we assume an oblate rotor shape, analysis of the data yields physically unrealistic, negative values for D_x and D_z that are not consistent between the one-photon and two-photon data. Based on these findings, we assert that NBDHA reorients as a prolate rotor in neat solvents, with $D_z/D_x \sim 2$.

With this information in hand, we now have a framework within which to evaluate NBDHA dynamics in solutions

containing unilamellar vesicles. A variety of unilamellar vesicle compositions were used to determine whether or not NBDHA interacts preferentially with a particular region of the bilayer. The addition of cholesterol and sphingomyelin to phospholipid vesicles is known to induce phase segregated regions within the bilayer structures [17]. Our recent work shows that varying the composition of bilayers does, in fact, influence the dynamics of the constituents (vide infra). The underlying question that the chromophore NBDHA addresses is the structural homology required of a probe molecule for it to locate within specific regions of the bilayer.

The steady state spectra of NBDHA in vesicles and in water are shown in Fig. 7. The absorption band maximum and shape is substantially different in water than in vesicle-containing solutions. NBDHA is not in the aqueous phase in vesicle-containing solutions. In water, NBD has a low quantum yield [54,55], and we were unable to detect a significant time-resolved fluorescence signal for NBDHA in water. NBDHA does not reside in the bulk water region of this system, and that for all vesicle-containing solutions the chromophore senses essentially the same environment.

When considering anisotropy decays for NBDHA in the presence of vesicles, we use the DSE (free rotor, Eq. (6)) model [48,50,51] instead of the hindered rotor model [46,47] based on the *ansatz* that the chromophore is bound to the surface of the unilamellar vesicles. We make this structural argument based on the steady-state data for NBDHA in vesicle-containing solutions and the fact that, for the lipids we use, there is a cationic quaternary ammonium species in closest proximity to the water at the lipid–solution interface. Because we make our measurements at pH 8, the NBDHA is fully deprotonated and, if the chromophore interacts with the vesicle, as suggested by the steady state absorption data, an ionic interaction would be likely. In this picture, the nominally tethered chromophore would experience a cone angle of $2\theta_0 \sim 180°$, which is a limiting case that renders the chromophore equivalent to a free rotor. For this reason, our reorientation data for NBDHA in the presence of vesicles are best modeled as free rotors rather than the hindered rotors.

We find that NBDHA reorients as a prolate rotor in the presence of vesicles. We have synthesized vesicles in a range of compositions, including the use of two different lipids with melting points substantially below (DLPC, mp = −1 °C) and substantially above (DSPC, mp = 55 °C) room temperature, and with the addition of cholesterol and sphingomyelin. Despite the wide range of environments within the vesicles that are available to NBDHA, we recover essentially the same one-photon excited reorientation times, regardless of vesicle composition (Table 4).

Treatment of the one-photon excited anisotropy decay times of NBDHA in vesicle-containing solutions in the context of a free rotor allows τ_{OR} to be related to the viscosity of the environment through the DSE equation (Eq. (6)), and the observation of single exponential anisotropy decays allows assignment of a prolate rotor shape to NBDHA in the presence of vesicles, based on our measurements of NBDHA in neat solvents (vide supra). Comparing the reorientation times of NBDHA in vesicle-containing solutions to the same data for NBDHA in neat solvents indicates that the local environment of NBDHA is characterized by a viscosity of ~1 cP, a value fully consistent with an aqueous environment. These data, in conjunction with the steady state data (Fig. 7), suggest that the probe resides in the polar headgroup region, in the immediate vicinity of the hydrophobic interior of the bilayer.

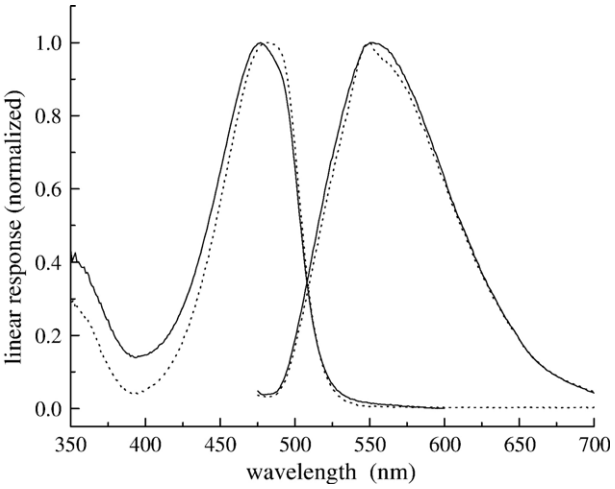

Fig. 7. Normalized absorption and emission spectra of NBDHA in neat water (dashed line) and in a solution containing DLPC vesicles (solid line). Spectra for all vesicle-containing solutions were identical.

With an understanding that NBDHA interacts with the polar headgroup region of bilayer structures, we study the behavior of other bilayer regions by using different probe molecules. We have used NBD-tagged cholesterol and a rhodamine-tagged phospholipid, and find that their transient responses individually as well as the excitation transport dynamics between them provides information on the extent of organization within different regions of the bilayer structure. Because sphingomyelin (SPM) is thought to play a role in forming cholesterol-rich bilayer regions, termed "lipid rafts," [17] we have explored the dynamics of these chromophores as a function of the amount of SPM in the bilayers.

The chemical information contained in fluorescence anisotropy measurements is in the form of the decay functionality of $R(t)$ (Eq. (2)). For these experiments the chromophores are tethered to membrane bilayer constituents, and we interpret the anisotropy data using the hindered rotor model [46,47]. For this model, the recovered anisotropy decay contains both an infinite-time anisotropy, $R(\infty)$, related to the steady-state restriction imposed on the chromophore by the presence of the bilayer, and a decay time constant, τ, related to the wobbling diffusion coefficient of the chromophore about its tethering bond. The bilayers we investigate are in the form of unilamellar vesicles (Fig. 2). For chromophores confined within a membrane, a steady state anisotropy is expected because of the restriction imposed by the membrane structure. Because the vesicles are spherical, the steady state anisotropy is orientationally averaged and we cannot observe the quantity $R(\infty)$. Also, the quantity τ in Eq. (4) contains contributions from both θ_0 and D_w. We place bounds on the value of D_w because it is the system-dependent changes in the quantity θ_0 that provide the structural information NBD-cholesterol. We estimate the diffusion coefficient for chromophore motion within

Table 4
Dependence of NBDHA anisotropy decay time constants and fluorescence lifetimes on vesicle composition

Vesicle system	τ_{OR} (ps)	τ_{fl} (ps)
DLPC	163±10	1173±88
DLPC/chol	166±4	1168±66
DLPC/chol/SPM	194±5	1177±62
DSPC	186±6	1144±45
DSPC/chol	176±6	1132±23
DSPC/chol/SPM	165±4	1145±44
DLPC/DSPC	159±6	1157±48
DLPC/DSPC/chol	161±8	1147±40
DLPC/DSPC/chol/SPM	186±5	1067±41

Abbreviations: DLPC = 1,2-Dilauroyl-*sn*-Glycero-3-Phosphocholine; DSPC = 1,2-Distearoyl-*sn*-Glycero-3-Phosphocholine; chol = cholesterol; SPM = sphingomyelin.

the cone to be similar to that of NBD-cholesterol in free solution, and calculate values of D from Eq. (6). This model provides reasonable predictions of experimental data.

We have studied the fluorescence lifetime and motional relaxation properties of NBD-cholesterol in unilamellar vesicles that contain DMPC, cholesterol, and controlled amounts of SPM and DMPE-rhodamine. For the simplest case, where there is no DMPE-rhodamine, and the SPM concentration is varied between 0 and 33 mol% of the total vesicle composition, we find that the NBD fluorescence lifetime decays as a single exponential and that there is no measurable dependence of the NBD motional relaxation time on SPM concentration.

We have also investigated the dependence of NBD-cholesterol (donor) lifetime and motional dynamics on the amount of DMPE-rhodamine (acceptor) within the bilayer structure. There is a marked acceptor concentration dependence in the NBD-cholesterol optical response, indicating not only communication between the chromophores, but also the structural influence of the DMPE-rhodamine molecule on the organization of the lipid regions of the bilayer. We show in Fig. 8 the fluorescence lifetime (s) and motional relaxation time of NBD-cholesterol as a function of DMPE-rhodamine, in the absence of SPM. The trends shown in Fig. 8 do not change with the addition of SPM, and we present these data as representative. The fluorescence lifetime data point to the interaction of the NBD and rhodamine chromophores, as expected. For low rhodamine concentrations, we observe a single fluorescence lifetime for NBD-cholesterol. As the acceptor concentration increases, we observe the onset of a two-component NBD fluorescence lifetime, with each lifetime exhibiting a concentration-dependence. This behavior is not consistent with a homogeneous system. We understand the two component NBD fluorescence population decay in the context of the DMPE-rhodamine either being in close proximity to a cholesterol-rich region of the bilayer (short lifetime) or relatively distant from any cholesterol-rich regions (long lifetime).

In an attempt to determine whether or not the cholesterol-rich regions exists as many small islands or as relatively large regions, we examined the NBD-cholesterol lifetime data in more detail (Fig. 8a). As the DMPE-rhodamine content of the bilayer is increased, we could expect one of three situations: a statistical distribution of DMPE-rhodamine chromophores in the lipid regions of the bilayer, preferential association of the DMPE-rhodamine with the cholesterol-rich bilayer regions, or aggregation of the DMPE-rhodamine species. In the first case, we expect that the NBD-cholesterol fluorescence lifetime would decrease monotonically with increasing DMPE-rhodamine composition, owing to the statistically determined variation in the critical transfer radius for the donor–acceptor pair. For the second case, we expect that the two NBD lifetime components would retain nominally the same time constants, but the fractional amount of the fast lifetime would increase with increasing DMPE-rhodamine concentration. For the third case, we would expect a decrease in the fractional contribution of the fast lifetime with increasing DMPE-rhodamine concentration because, as DMPE-rhodamine is added, aggregation would occur, effectively reducing the amount of acceptor available for excitation transport. We show in Fig. 9 that this is the case, where the fractional contribution of the short fluorescence lifetime decreases with increasing acceptor concentration. Both the fast and slow NBD-cholesterol lifetimes decrease

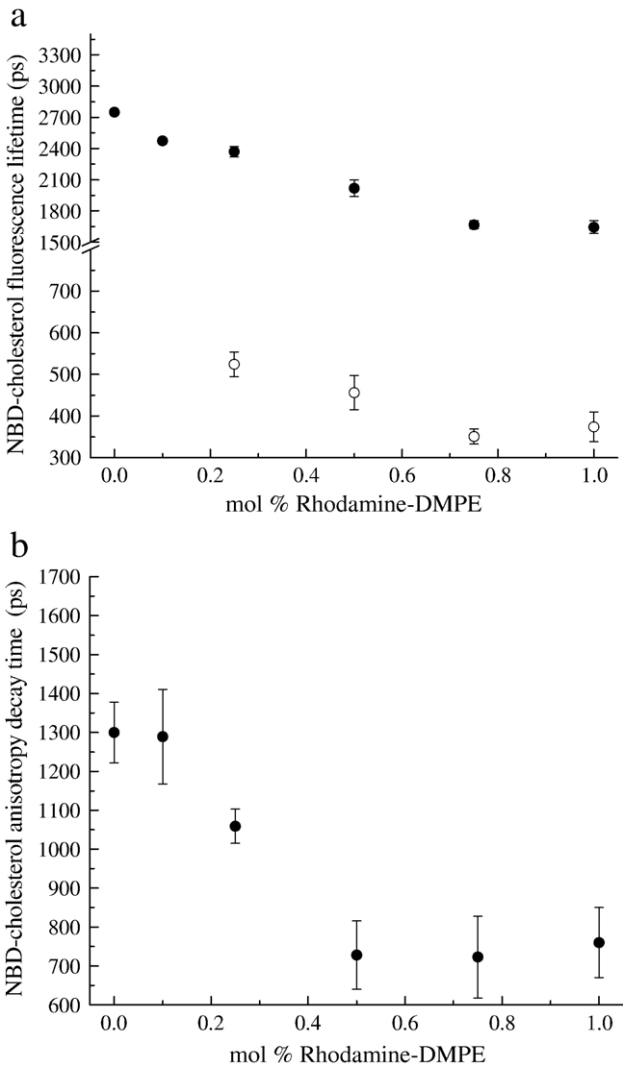

Fig. 8. Changes in (a) lifetime and (b) reorientation time of NBD-cholesterol with increasing DMPE-rhodamine concentration, from 0 to 1 mol%, with a constant concentration of 0 mol% SPM.

monotonically with increasing DMPE-rhodamine content due to the expected Förster donor–acceptor coupling between NBD-cholesterol and non-aggregated DMPE-rhodamine within the bilayer.

The motional relaxation behavior of NBD-cholesterol does not depend significantly on the bilayer SPM content, but does depend on the amount of optical acceptor present (Fig. 8b). We understand the change in NBD-cholesterol dynamics as an increase in the organization of the cholesterol-rich region with the addition of DMPE-rhodamine. The measured anisotropy decay time constant, τ, increases with the volume accessible to the chromophore. In estimating D_w, the limiting factor is knowing the viscosity experienced by the chromophore. Early estimates of the viscosity of lipid bilayer systems were on the order of 100 cP [56]. Among the issues contributing to uncertainty in estimates of bilayer viscosity has been the composition of the bilayer. Work in our lab on the rotational diffusion of perylene in bilayers points to the viscosity of the systems we report on here being in the range of 10–20 cP [57]. Given this viscosity range, we can bound the value of $D \sim D_w$ for NBD-cholesterol (Table 2). Using the range of calculated D_w values for these chromophores, we infer system-dependent variations in the confining cone-angle (Table 3).

Our experimental data point to a decrease in motional freedom for NBD-cholesterol with increasing DMPE-rhodamine concentration. As the concentration of DMPE-rhodamine increases, the NBD-cholesterol experiences a step-wise change in its motional freedom, losing on the order of 20% of its available cone angle ($2\theta_0$) in the motionally-restricted regime. These data are not consistent with a direct complexation of NBD-cholesterol with aggregates of DMPE-rhodamine because the dynamics of the two chromophores exhibit two distinctly different bilayer composition dependencies (vide infra).

The hypothesis of DMPE-rhodamine homo-aggregation can be tested by examining the dynamics of this chromophore as a function of its concentration (Fig. 10). For low DMPE-rhodamine concentrations we observe $\tau \sim 150$ ps, and as the concentration of DMPE-rhodamine is increased, τ increases to ~650 ps and remains at this value. Because of the location of the rhodamine chromophores, the system-dependent variations in τ are dominated by changes in D_w rather than θ_0. We interpret our data in this manner because the attractive interactions holding the lipid head groups in place are less amenable to large amplitude separation than are the nonpolar organic region(s) within the bilayer region. The increase in DMPE-rhodamine motional relaxation time reflects aggregation rather than an increase in motional freedom. The DMPE-rhodamine chromophore exists at the interface between the lipid polar head groups and the water solvent. In this model, aggregation would occur once the concentration of the chromophore was sufficiently high, and the resulting aggregated regions within the bilayer structure would be more rigid than the "free" lipid regions. The experimental lifetime and motional relaxation data for DMPE-rhodamine are fully consistent with the aggregation of this species.

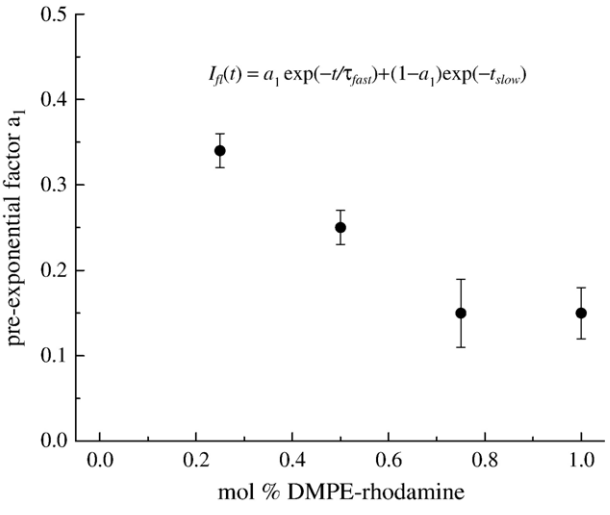

Fig. 9. The fractional contribution of the fast fluorescent lifetime component of NBD-cholesterol as a function of DMPE-rhodamine concentration.

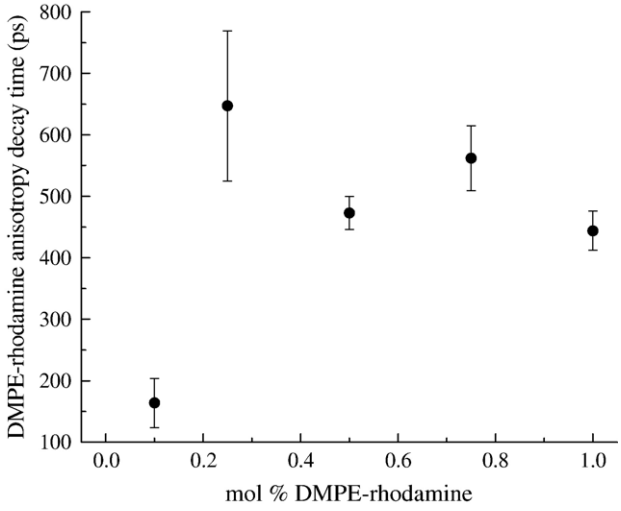

Fig. 10. Dependence of DMPE-rhodamine anisotropy decay time on DMPE-rhodamine concentration (11 mol% SPM fixed for all measurements).

The NDB-cholesterol motional relaxation data are also consistent with the aggregation of DMPE-rhodamine in the lipid regions of the bilayer. The experimental data for NBD-cholesterol indicate that as the concentration of DMPE-rhodamine increases, the cholesterol-rich regions become better ordered. These data point to the presence of the DMPE-rhodamine in the lipid regions of the bilayer effectively making the entire bilayer structure more rigid, thereby reducing the mobility of the cholesterol-rich bilayer regions.

4. Conclusions

As noted in the Introduction, there are several key elements to the creation of a sensing device based on biomolecular recognition or processes. We have discussed our progress toward creating a well understood interface between the biomolecule sensing agent of interest and the signal transducing substrate/support. There is a range of monolayer interfacial modification chemistry that can be applied to the transducer surface and we have characterized organization and electron transfer within this layer for a range of systems. We have also studied the bilayers that

will be required to support biomolecules on the monolayer-modified transducer. Our work highlights the highly interactive nature of different regions of heterogeneous bilayer structures and demonstrates that with the addition of the appropriate components to the bilayers we can control the fluidity of these systems. Gaining control over interface fluidity is a critical step in making these systems useful for supporting essentially any biomolecule, and future work will center on tuning bilayer properties for specific applications.

Acknowledgment

This work was supported by the National Science Foundation Grant 0445492 and the Ministry of Scientific Research and Information Technology in 2004–2007, Project No. PBZ 18-KBN098/T09/2003. The NSF-PAS mobility grant is also gratefully acknowledged.

References

[1] R.G. Nuzzo, D.L. Allara, Adsorption of bifunctional organic disulfides on gold surfaces, J. Am. Chem. Soc. 105 (1983) 4481–4483.
[2] D.S. Karpovich, G.J. Blanchard, Direct measurement of the adsorption kinetics of alkanethiolate self-assembled monolayers on a microcrystalline gold surface, Langmuir 10 (1994) 3315–3322.
[3] H.M. Schessler, D.S. Karpovich, G.J. Blanchard, Quantitating the balance between enthalpic and entropic forces in alkanethiol/gold monolayer self assembly, J. Am. Chem. Soc. 118 (1996) 9645–9651.
[4] P. Kohli, G.J. Blanchard, Applying polymer Chemistry to interfaces: layer-by-layer and spontaneous growth of covalently bound multilayers, Langmuir 16 (2000) 4655–4661.
[5] J.S. Major, G.J. Blanchard, Strategies for covalent multilayer growth. 2. Interlayer linking chemistry, Chem. Mater. 14 (2002) 2574–2581.
[6] D.C. Dong, M.A. Winnik, The py scale of solvent polarities. Solvent effects on the vibronic fine structure of pyrene fluorescence and empirical correlations with E_T and Y Values, Photochem. Photobiol. 35 (1982) 17–21.
[7] D.C. Dong, M.A. Winnik, The py scale of solvent polarities, Can. J. Chem. 62 (1984) 2560–2565.
[8] J.W. Carr, J.M. Harris, Fluorescence studies of the stationary-phase chemical environment in reversed-phase liquid chromatography, Anal. Chem. 58 (1986) 626–631.
[9] J.W. Carr, J.M. Harris, Temperature-induced changes in reversed-phase chromatographic surfaces: C8 and C9 polymeric ligands, J. Chromatogr. 481 (1989) 135–146.
[10] R.G. Bogar, J.C. Thomas, J.B. Callis, Lateral diffusion of solutes bound to the alkyl surface of C18 reversed-phase liquid chromatographic packings, Anal. Chem. 56 (1984) 1080–1084.
[11] E. Wistus, E. Mukhtar, M. Almgren, S.E. Lindquist, Behavior of pyrene in air/water monolayers of eicosanoic acid, Langmuir 8 (1992) 1366–1371.
[12] Y.S. Liu, W.R. Ware, Photophysics of polycyclic aromatic hydrocarbons adsorbed on silica gel surfaces. 1. Fluorescence lifetime distribution analysis: an ill-conditioned problem, J. Phys. Chem. 97 (1993) 5980–5986.
[13] Y.S. Liu, P. de Mayo, W.R. Ware, Photophysics of polycyclic aromatic hydrocarbons adsorbed on silica gel surfaces. 2. Lifetime distribution and symmetry, J. Phys. Chem. 97 (1993) 5987–5994.
[14] Y.S. Liu, P. de Mayo, W.R. Ware, Photophysics of polycyclic aromatic hydrocarbons adsorbed on silica gel surfaces. 3. Fluorescence quantum yields and radiative decay rate constants derived from lifetime distributions, J. Phys. Chem. 97 (1993) 5995–6001.
[15] D.S. Karpovich, G.J. Blanchard, Relating the polarity-dependent fluorescence response of pyrene to vibronic coupling. Achieving a fundamental understanding of the py polarity scale, J. Phys. Chem. 99 (1995) 3951–3958.
[16] M. Mazur, G.J. Blanchard, Photochemical and electrochemical oxidation reactions of surface-bound polycyclic aromatic hydrocarbons, J. Phys. Chem., B 108 (2004) 1038–1045.
[17] K. Simons, G. van Meer, Lipid sorting in epithelial cells, Biochemistry 27 (1988) 6197–6202.
[18] P. Krysiński, M. Brzostowska-Smolska, Three-probe voltammetric characterisation of octadecanethiol self-assembled monolayer integrity on gold electrodes, J. Electroanal. Chem. 424 (1997) 61–67.
[19] J. Izdebski, Preparatyka i elementy syntezy organicznej 17 (1983), 836.
[20] A.J. Driessen, H.W. van den Hooven, W. Kuiper, M. van de Kamp, H.G. Sahl, R.N. Konings, W.N. Konings, Mechanistic studies of lantibiotic-induced permeabilization of phospholipid vesicles, Biochemistry 34 (1995) 1606–1614.
[21] L.D. Mayer, M.J. Hope, P.R. Cullis, Vesicles of variable sizes produced by a rapid extrusion procedure, Biochim. Biophys. Acta 858 (1986) 161–168.
[22] E.C. Unger, P. MacDougall, P. Cullis, C. Tilcock, Liposomal gadoliniumDTPA: effect of encapsulation on enhancement of hepatoma model by MRI, Magn. Reson. Imaging 7 (1989) 417–423.
[23] D.G. Hunter, B.J. Frisken, Effect of extrusion pressure and lipid properties on the size and polydispersity of lipid vesicles, Biophys. J. 74 (1998) 2996–3002.
[24] R.C. MacDonald, R.I. MacDonald, B.P. Menco, K. Takeshita, N.K. Subbarao, L.R. Hu, Small–volume extrusion apparatus for preparation of large, unilamellar vesicles, Biochim. Biophys. Acta 1061 (1991) 297–303.
[25] N.K. Subbarao, R.I. MacDonald, K. Takeshita, R.C. MacDonald, Characteristics of spectrininduced leakage of extruded, phosphatidylserine vesicles, Biochim. Biophys. Acta 1063 (1991) 147–154.
[26] L. Dewitt, G.J. Blanchard, E. Legoff, M.E. Benz, J.H. Liao, M.G. Kanatzidis, Determination of ground–and excited–state isomerization barriers for the oligothiophene 3′,4′–dibutyl–2, 2′:5',2″–terthiophene, J. Am. Chem. Soc. 115 (1993) 12158–12164.
[27] E.J. Moriconi, B. Rakoczy, W.F. O'Connor, Oxidation–reduction potentials and absorption spectra of polycyclic aromatic quinones, J. Org. Chem. 27 (1962) 2772–2776.
[28] M. Dominska, K. Jackowska, P. Krysinski, G.J. Blanchard, Probing interfacial organization in surface monolayers using tethered pyrene. 1. Structural mediation of electron and proton access to adsorbates, J. Phys. Chem., B 109 (2005) 15812–15821.
[29] A.B. Serfis, S. Brancato, S.J. Fliesler, Comparative behavior of sterols in phosphatidylcholine-sterol monolayer films, Biochim. Biophys. Acta 1511 (2001) 341–348.
[30] J.G. Gordillo, D.J. Schiffrin, The electrochemistry of ubiquinone-10 in a phospholipid model membrane, Faraday Discuss. 116 (2000) 89–108.
[31] M.R. Moncelli, R. Herrero, L. Becucci, R. Guidelli, Kinetics of electron and proton transfer to ubiquinone-10 and from ubiquinol-10 in a self-assembled phosphatidylcholine monolayer, Biochim. Biophys. Acta 1364 (1998) 373–384.
[32] M.R. Moncelli, L. Becucci, A. Nelson, R. Guidelli, Electrochemical modeling of electron and proton transfer to ubiquinone-10 in a self-assembled phospholipid monolayer, Biophys. J. 70 (1996) 2716–2726.
[33] S.E. Creager, T.T. Wooster, A new way of using ac voltammetry to study redox kinetics in electroactive monolayers, Anal. Chem. 70 (1998) 4257–4263.
[34] S. Creager, C.J. Yu, C. Bamdad, S. O'Connor, T. MacLean, E. Lam, Y. Chong, G.T. Olsen, M. Gozin, J.F. Kayyem, Electron transfer at electrodes through conjugated "molecular wire" bridges, J. Am. Chem. Soc. 121 (1999) 1059–1064.
[35] J.J. Sumner, S.E. Creager, Redox kinetics in monolayers on electrodes: Electron transfer is sluggish for ferrocene groups buried within the monolayer interior, J. Phys. Chem., B 105 (2001) 8739–8745.
[36] S. Sek, A. Sepiol, A. Tolak, A. Misicka, R. Bilewicz, Distance dependence of the electron transfer rate through oligoglycine spacers introduced into self-assembled monolayers, J. Phys. Chem., B 108 (2004) 8102–8105.
[37] C.D. Bain, E.B. Troughton, Y.T. Tao, G.M. Whitesides, R.G. Nuzzo, Formation of monolayer films by the spontaneous assembly of organic thiols from solution onto gold, J. Am. Chem. Soc. 111 (1989) 321–335.
[38] J.J. Sumner, K.S. Weber, L.A. Hockett, S.E. Creager, Long-range heterogeneous electron transfer between ferrocene and gold mediated by

n-alkane and *N*-alkyl-carboxamide bridges, J. Phys. Chem., B 104 (2000) 7449–7454.
[39] S. Sek, B. Palys, R. Bilewicz, Contribution of intermolecular interactions to electron transfer through monolayers of alkanethiols containing amide groups, J. Phys. Chem., B 106 (2002) 5907–5914.
[40] K. Weber, L. Hockett, S. Creager, Long-range electronic coupling between ferrocene and gold in alkanethiolate-based monolayers on electrodes, J. Phys. Chem., B 101 (1997) 8286–8291.
[41] A.M. Napper, H. Liu, D.H. Waldeck, The nature of electronic coupling between ferrocene and gold through alkanethiolate monolayers on electrodes: The importance of chain composition, interchain coupling, and quantum interference, J. Phys. Chem., B 105 (2001) 7699–7707.
[42] J.J. Tulock, G.J. Blanchard, Investigating hydrolytic polymerization of aqueous zirconium ions using the fluorescent probe pyrenecarboxylic acid, J. Phys. Chem., B 106 (2002) 3568–3575.
[43] P. Krysinski, G.J. Blanchard, Synthesis and characterization of amphiphilic biomimetic assemblies at electrochemically active surfaces, Langmuir 19 (2003) 3875–3882.
[44] L. Kelepouris, P. Krysinski, G.J. Blanchard, Gauging molecular interactions between substrates and adsorbates. Substrate mediation of surface-bound chromophore vibronic coupling, J. Phys. Chem., B 107 (2003) 4100–4106.
[45] D.S. Karpovich, G.J. Blanchard, Dynamics of a tethered chromophore imbedded in a self-assembled monolayer, Langmuir 12 (1996) 5522–5524.
[46] A. Szabo, Theory of fluorescence depolarization in macromolecules and membranes, J. Chem. Phys. 81 (1984) 150–167.
[47] G. Lipari, A. Szabo, Effect of vibrational motion on fluorescence depolarization and nuclear magnetic-resonance relaxation in macromolecules and membranes, Biophys. J. 30 (1980) 489–506.
[48] P. Debye, Polar Molecules, Chemical Catalog Co., New York, 1929.
[49] T.J. Chuang, K.B. Eisenthal, Theory of fluorescence depolarization by anisotropic rotational diffusion, J. Chem. Phys. 57 (1972) 5094–5097.
[50] F. Perrin, Brownian movement of an ellipsoid (II). Free rotation and depolarisation of fluorescences. Translation and diffusion of ellipsoidal molecules, J. Phys. Radium 7 (1936) 1–11.
[51] R. Zwanzig, A.K. Harrison, Modifications of the Stokes–Einstein formula, J. Chem. Phys. 83 (1985) 5861–5862.
[52] J.T. Edward, Molecular volumes and Stokes–Einstein equation, J. Chem. Educ. 47 (1970) 261–270.
[53] J.L. Dela Cruz, G.J. Blanchard, Reorientation dynamics of rhodamine 640 in normal alcohols: measurement of the length and time scale of transient local heating in solution, J. Phys. Chem., A 105 (2001) 9328–9835.
[54] S. Fery-Forgues, J.-P. Fayet, A. Lopez, Drastic changes in the fluorescence properties of NBD probes with the polarity of the medium—involvement of a TICT state, J. Photochem. Photobiol., A Chem. 70 (1993) 229–243.
[55] S. Lin, W.S. Struve, Time-resolved fluorescence of nitrobenzoxadiazole aminohexanoic acid—effect of intermolecular hydrogen-bonding on non-radiative decay, Photochem. Photobiol. 50 (1991) 361–365.
[56] M. Edidin, Lipids on the frontier: a century of cell-membrane bilayers, Nat. Rev. 4 (2003) 414–418.
[57] M.M. Koan, G.J. Blanchard, Rotational dynamics of perylene in unilamellar lipid vesicles. Quantitating the role of structural defects on bilayer fluidity, J. Phys. Chem., B (in press).